Applied Physics, Material Sciences, and Engineering Journal
ISSN 3065-1425
Volume 13 Issue 1
January-March 2025
Impact Factor: 8.13
Enquiry: contact@continentalpub.online
Published by Continental Publication | https://cspjournals.org/index.php/apmsej

CHARGE TRANSPORT BEHAVIOR IN NATURAL SEPIA MELANIN NANOGRANULES

Amara Louise Ndiaye
Department of Engineering Physics, Polytechnique Montreal, 2500 Ch. de Polytechnique, Montreal, QC, H3T 1J4, Canada

Abstract: *Sepia eumelanin, a natural biopigment extracted from cuttlefish ink, has attracted growing interest as a sustainable material for organic electronics. Its nanogranular structure, composed of DHI and DHICA monomers, presents unique charge transport characteristics influenced by hydration and measurement scale. While prior studies have explored its mixed ionic–electronic conductivity at micro- and millimetric ranges, the intrinsic electronic properties at the nanoscale remain underexplored. In this study, we investigate the nanoscale charge transport behavior of Sepia melanin using e-beam lithography-fabricated electrodes with submicron separations. Through current–voltage, current–time, and electrochemical impedance spectroscopy measurements, we observed predominantly electronic transport mechanisms, with conductivity increasing at smaller interelectrode distances. Temperature-dependent analysis enabled extraction of activation energy values, further elucidating the transport processes. These findings underscore the relevance of distance scale in assessing the true conductive potential of natural materials and support Sepia melanin's viability in bio-inspired electronic applications.*

Keywords: *Sepia melanin, nanoscale transport, organic electronics, charge conductivity*

1. Introduction

Nature provides a wonderful source of materials for sustainable technologies across various fields, including electronics, photonics, energy, and biomedical [1–5]. Natural (bio-sourced) organic materials with conjugated molecular structures are attractive for sustainable organic electronics for a number of reasons:
they do not require lab synthesis, they permit to limit the use of critical elements and are potentially biodegradable [6–11]. Biodegradability is relevant if we think of electronic waste, which reached 62 megatons globally in 2022 and is projected to reach 82 megatons by 2030 [12]. Additionally, organic materials can be solution-processed, thus opening the possibility of reducing the device embodied energy compared to conventional high-temperature, high-vacuum methods [13]. It is worth noticing that bio-sourced organic materials typically exhibit complex chemical compositions, including salts, contributing to structural and energetic disorder and affecting charge transport.

Vol. 13 No. 1 | Imp. Factor: 8.13
DOI: https://doi.org/10.5281/zenodo.15845904
Eumelanin, the black–brown member of the melanin family, has been studied for its moisture-dependent electrical response, redox activity, broadband optical absorption, metal chelation, and free-radical scavenging properties [14–16].

Eumelanin develops hierarchically from the (5, 6)-dihydroxyindole (DHI) and (5, 6)dihydroxyindole2-carboxylic acid (DHICA) building blocks (monomers). DHI and DHICA have multiple polymerization sites and can therefore give different oligomers, of different sizes. Oligomers of both DHI and DHICA

assemble hierarchically through π–π stacking to form protomolecules of about 4–5 planes, with an interplanar distance of approximately 3.5 Å, and a lateral extension of about 20 Å [14, 17, 18]. In turn, these protomolecules form 10 to 15 nm-sized structures by π–π stacking and edge-to-edge H-bonding interactions. The same physical interactions are responsible of the formation of larger spherical granules ranging from 100 to 300 nm [14]. High-resolution atomic force microscopy has revealed protrusions developing from the spherical granules, attributable to sub-granular structures in eumelanin; average width and height of protrusions are ~19 nm and ~3 nm, respectively [18].

McGinness *et al* [19] reported on the resistive electrical switching in wet eumelanin pellets in the 1970 s and explained it through the amorphous semiconductor model. This explanation was later challenged by Mostert *et al*, who proposed a mixed protonic–electronic transport mechanism based on electrical, muon spin relaxation, and electron paramagnetic resonance measurements [20, 21]. Recent studies on Sepia eumelanin (henceforth indicated as Sepia melanin) have shown predominant electronic transport in dry pellets [15] and printed films incorporating insulating binders [6, 22]. Such studies have probed interelectrode distances from 10 μm to 2 mm.

In this work, we study the electrical response of Sepia melanin at the nanometric scale, using e-beam lithography (EBL)-patterned metal contacts (interelectrode distances of 400 and 700 nm). Studies at the nanoscale are needed to capture the charge transport behavior at the scale of small clusters of granules. Our hypothesis is that, by narrowing down the interelectrode distance, we reduce the number of granules within the interelectrode region and, consequently, the number of inter-granules' boundaries between them, in turn getting closer to the upper, intrinsic (boundary-free) limit of the electrical conductivity of Sepia melanin. After a scanning electron microscopy (SEM) survey of the material deposited on electrode-patterned SiO_2/Si, we measured the electrical response of Sepia melanin in ambient conditions (by current–voltage, current–time in potentiostatic conditions, impedance spectroscopy). By conducting temperature-dependent electrical measurements, we deduced the activation energy for charge carrier transport. Our work on Sepia melanin at the nanoscale advances the knowledge on the functional properties of bio-sourced organic electronic materials for their rational use in technologies and devices with low environmental footprint such as moisture sensors, photoconductors, and biodegradable supercapacitors.

2. Materials and methods

2.1. Materials for extraction of Sepia melanin

Sepia officinalis cuttlefish ink (Stareef Seafood Boston, a product of Spain) was purchased from a fish market in Montreal. Hydrochloric acid (HCl, ACS Reagent 37%) was acquired from Acros Organics. Monobasic sodium phosphate, dibasic sodium phosphate solution (0.5 M in H_2O), ethanol (ACS

Vol. 13 No. 1 | Imp. Factor: 8.13
DOI: https://doi.org/10.5281/zenodo.15845904

reagent 99.8%), ethyl acetate, 1-propanol (⩾99.5%), and 1-methoxy-2-propanol (⩾99.5%) were obtained from Sigma-Aldrich.

2.2. Sepia melanin powders extraction and purification

Sepia melanin powders were obtained from the commercial ink of *Sepia officinalis* using a method modified from previously documented extraction procedures [7, 15, 22, 23]. In summary, 300 g of commercial cuttlefish ink were suspended in 500 ml of 2 M HCl and stirred for 24 h at room temperature. Following the stirring process, the slurry underwent centrifugation (Allegra-X30R Centrifuge, Beckman Coulter) followed by: three successive washes with 0.5 M HCl, and single washings with de-ionized (DI) water, a buffer solution (0.02% vol/vol monobasic sodium phosphate 200 mM, 32.49% vol/vol dibasic sodium phosphate 200 mM, and 67.49% vol/vol of DI water), ethanol, DI water, and ethyl acetate. Lastly, the slurry underwent four additional washes with DI water. Each centrifugation step was conducted at 10 000 rpm, 5 °C, with varying durations (15 min for HCl 2 M, HCl 0.5 M, ethanol, and ethyl acetate and 25 min for the buffer solution and DI water). The resulting product underwent lyophilization at 80 °C for 24 h to remove residual DI water, yielding a fine black Sepia melanin powders. This extraction process achieved a yield ranging from approximately 10% to 12% in weight, exemplified by obtaining around 30–35 g of powder from 300 g of cuttlefish ink.

2.3. Suspension of extracted Sepia melanin in methanol

Interdigitated patterns with Au-electrodes on SiO_2/Si substrates were cleaned by sequential sonication in acetone, isopropanol and DI water during 15 min for each step, followed by 10 min UV-ozone treatment before drop-casting the suspension of Sepia melanin. We prepared the suspension of Sepia melanin in methanol at a concentration of 1 mg ml^{-1} (no stirring or heating involved). The mixture was sonicated for 20 min. The purity of the methanol (grade: for HPLC) that we used to make the suspension of Sepia melanin was 99.9%. The suspension was left at rest for about 30 min, prior drop casting. A volume of 10 μl of suspension was drop-cast on interdigitated patterns. Drop cast samples were left drying for 10 min in ambient conditions without any heat treatment, for methanol to evaporate. We measured around 15 samples for each interelectrode distance. We run SEM experiments (imaging) over 5 samples for each interelectrode distance. Results are reproducible in terms of conductivity; the intensity of the current depends on the *effective* channel width covered by Sepia melanin.

2.4. Patterning of the electrodes by EBL

SiO_2/Si substrates (Si thickness 525 ± 25 μm, oxide thickness 200 ± 10 nm) were cleaned by sequential sonication in acetone, isopropanol and DI water for 15 min each, followed by 10 min UV-ozone treatment. To deposit the double layer of polymethyl methacrylate (PMMA) resist, firstly the resist PMMA495A4 was spin-coated (3000 rpm, 30 s, h = 150 nm), followed by a soft bake on a hot plate for 180 s at 180 °C. Afterwards, PMMA950A2 resist was spin-coated (3000 rpm, 30 s, h = 50 nm) followed by a soft bake on hot plate for 180 s at 180 °C, again. The interdigitated patterns with interelectrode distance L = 700 and 400 nm were created using the e-Line Plus software and fabricated by EBL as described below. Substrates were initially exposed to the e-beam (working distance = 10 mm, aperture = 30 μm, applied voltage = 10 kV, beam current ~0.2 nA). Afterwards, they were developed by immersion in a developer solvent mixture made up of methyl isobutyl ketone and isopropanol alcohol

Vol. 13 No. 1 | Imp. Factor: 8.13
DOI: https://doi.org/10.5281/zenodo.15845904

(MIBK and IPA in a ratio of 1:3), for 50 s followed by immersion of the substrate in IPA and DI water for 30 s each. The substrates were ultimately rinsed with DI water and dried using an N_2 gun.

2.5. Metal deposition

After development, metal deposition was done by physical vapor deposition in an electron-beam evaporation chamber with a vacuum level of 10^{-6} Torr. The thickness of the metal layers, including a 5 nm-thick titanium adhesion layer and a subsequent 50 nm-thick Au layer, was precisely controlled using a quartz microbalance (deposition rate 0.6 Å s^{-1}). Then, the lift-off process involved immersing the substrate in acetone for 24 h, followed by rinsing with DI water and drying using an N_2 gun. Subsequently, before depositing the Sepia melanin, the substrates underwent a cleaning process like the pre-patterning cleaning procedure.

2.6. Morphology

The morphology of Sepia melanin was investigated on SiO_2/Si by ESEM (QUATTRO microscope, backscattering mode, voltage 1 kV and 5 kV and pressure ~10^{-3} Pa).

2.7. Electrical characterizations

Sepia melanin granules were deposited onto 1 cm × 1 cm SiO_2/Si substrates patterned with interdigitated Au-patterned electrodes (consisting of a 5 nm-thick Ti adhesion layer and 50 nm of Au, featuring an interelectrode distance L of 700 and 400 nm) using the drop-casting method. Current (I)–voltage (V) and current (I)–time (t) measurements were conducted under ambient conditions on Sepia melanin drop-casted onto 1 cm × 1 cm Au-patterned SiO_2/Si electrodes using an Agilent B1500 semiconductor analyzer. I–V characteristics were collected at a scan rate of 50 mV s^{-1}. Temperature-dependent electrical response of drop-casted Sepia melanin granules was acquired in vacuum on Au-patterned interdigitated electrodes on SiO_2/Si substrate in a cryogenic micromanipulated optoelectronic probe station (CPX Lakeshore) equipped with a heating stage (10^{-7} Torr, from 295 K to 380 K at steps of 10 K). The electrical conductivity of Sepia melanin was determined based on the I–V (current–voltage) response using the following method:

$$\sigma = \frac{L}{RA}$$

where L is the interelectrode distance (700 and 400 nm), R is the Sepia melanin's resistance (including the contact resistance) measured at an applied voltage V = 1 V and V = 0.5 V for an interelectrode distance of 700 and 400 nm (SI, table S2) respectively, and A is the cross-sectional area (*effective* channel width × thickness of the sample which are 205 μm × 300 nm for 700 nm interelectrode distance and 450 μm × 300 nm for 400 nm interelectrode distance, respectively) (SI, table S1). To deduce the effective width, we used the software ImageJ (https://imagej.net/ij). To calculate the conductivity, we took thickness of Sepia melanin granules as 300 nm (diameter of largest granule).

2.8. Electrochemical impedance spectroscopy (EIS)

EIS data were collected at open circuit potential within the frequency range of 3 MHz to 1 Hz, with 10 data points per decade and a 100 mV oscillation amplitude. A multichannel potentiostat (Biologic, model VSP 300) was employed for the data collection.

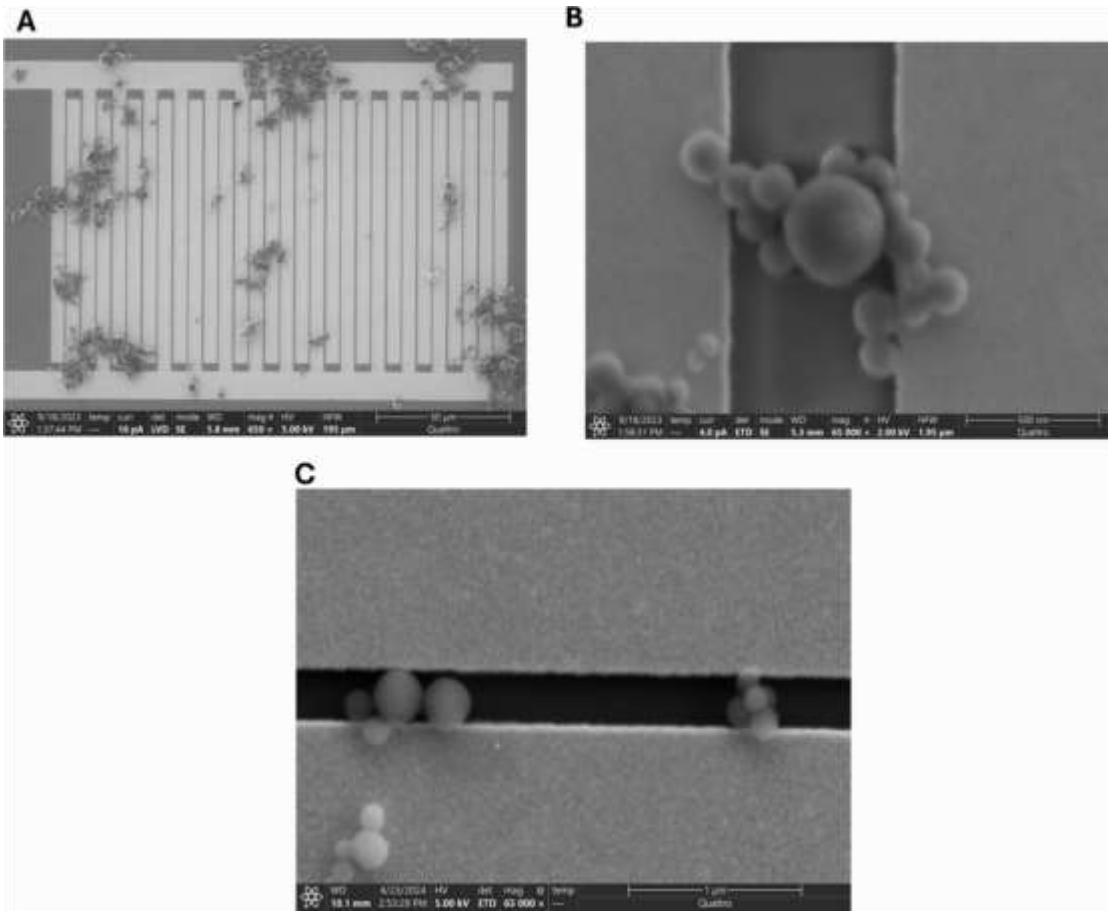

Figure1. SEM images of Sepia melanin's granules on interdigitated Au/Ti electrode-patterned SiO_2/Si substrates. Images in (A), and (B) are obtained on substrates patterned with an interelectrode distance of 700 nm whereas (C) with 400 nm.

3. Results and discussion

SEM images of Sepia melanin, drop-cast from a methanol suspension onto Au electrode-patterned SiO_2/Si substrates with interelectrode distances of 700 nm and 400 nm, show that the diameter of the Sepia melanin's granules lies in the range 100–300 nm, in agreement with the literature (figure 1) [18]. SEM images show that Sepia melanin granules cover only a limited portion of the substrate (figure 1(A)). For the interelectrode distances probed in this work, SEM images show that granules can be in physical contact to form continuous paths bridging the interelectrode distance (figures 1(B) and (C)). Further, for large granules and short interelectrode distances (400 nm), one individual Sepia melanin granule can bridge the interelectrode distance (figure 1(C)).

Current–voltage (I–V) plots obtained in ambient conditions for Sepia melanin samples with an interelectrode distance of 700 nm show that the current increases with the voltage, from 0 to 1 V (figure 2(A)). At low voltages (0–0.5 V), I–V plots exhibit an ohmic behavior [6]. However, at higher voltages (0.5–1 V), plots follow a power law $I \alpha V^a$ (figure 2(A)), indicating a non-ohmic behavior.

Log(J)–log(V) plots (where J is the current density) indicate a transition in slope from an ohmic regime with $a = 1.002 \pm 0.002$ to a non-ohmic regime, with $a = 1.329 \pm 0.005$ (SI, figure S2) [24].

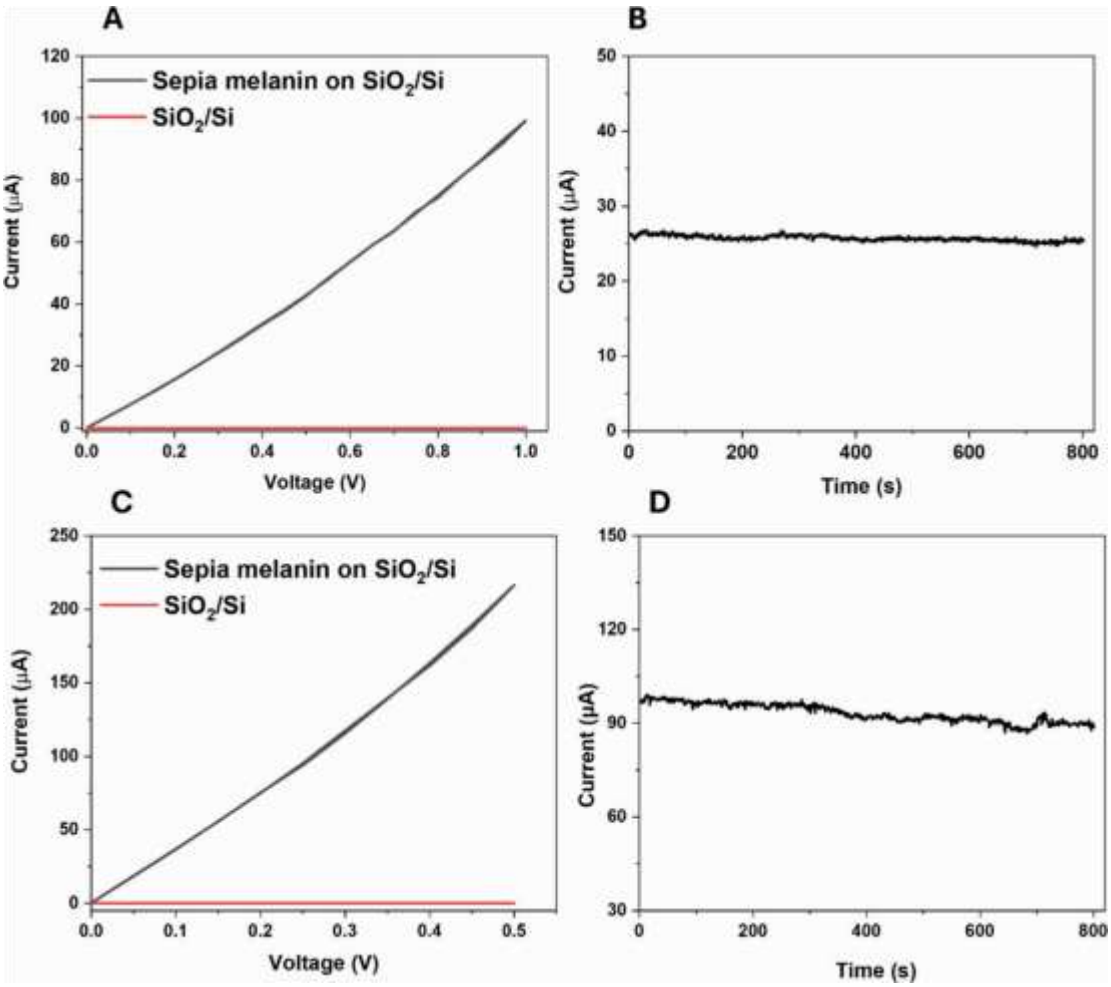

Figure2. Electrical response of Sepia melanin on Au/Ti interdigitated-electrode-patterned SiO_2/Si, in ambient conditions. (A) *I–V* and (B) *I–t* at 0.3 V, for 700 nm. (C) *I–V* and (D) *I–t* at 0.3 V for 400 nm. The response of the bare SiO_2/Si substrate is included in (A) and (C).

We tentatively explain the power law behavior as follows. Upon application of an electrical bias, charge carriers are injected in Sepia melanin, bringing about the formation of an electronic space-charge layer at the Sepia melanin/metal interface [15, 22]. The formation of space-charge layers is caused by the presence of electronic traps, in turn due to structural disorder present in Sepia melanin, including at its interface with the metal electrodes. Upon application of sufficiently high biases, trap filling would lead to the observed power-law behavior [25–27].

An analogous behavior in the *I–V* plots was observed for the interelectrode distance of 400 nm, where we observed an ohmic behavior in the region 0–0.3 V and a non-ohmic one in the region 0.3–0.5 V (figure 2(C)). The ohmic-to-non-ohmic transition occurs approximately at the same electric field (i.e. 7×10^5 V m^{-1}), for interelectrode distances. Similar transitions have been reported in the literature with dry Sepia melanin pellets [15] and Sepia melanin-based printed films [22].

Current–time (*I–t*) characteristics, obtained upon application of a constant voltage of 0.3 V to Sepia melanin samples, exhibit a plateau-like behavior, for both types of samples, i.e. 700 and 400 nm interelectrode distances (figures 2(B) and (D)). The presence of plateaus in the *I–t* plots suggests that

electronic transport is the dominant mode of conduction in the samples. Indeed, when both electronic and ionic transport occur between ion-blocking electrodes [16] (as is the case for our Au/Ti electrodes), *I–t* plots display an initial exponential decay associated to the formation of ionic electrical double layers at the Sepia melanin/metal electrode interface, followed by a plateau attributable to electronic transport [15, 16].

Electronic conductivity was calculated by evaluating the area covered by Sepia melanin (SI, figure S1, table S1).

Considering the *effective* (i.e. covered by Sepia melanin) channel width and, as sample thickness, the thickness (i.e. diameter) of one granule of Sepia melanin (see materials and methods), we obtained conductivity values of $0.95 \pm 0.01 \times 10^{-2}$ S cm^{-1} and $1.55 \pm 0.01 \times 10^{-2}$ S cm^{-1} for 700 and 400 nm interelectrode distances, respectively. The higher conductivity observed when the interelectrode distance was reduced from 700 to 400 nm may be attributed to the decreased number of inter-granules' boundaries.

EIS was employed to understand the dynamics of charge transfer and charge carrier transport [28]. The Nyquist plot, showing the imaginary part of the impedance (–Im [*Z*]), against its real part (Re [*Z*]), shows a semicircle (figure 3(A)). The diameter of this semicircle is associated with the electronic resistance of the Sepia melanin. The observation of a single semicircle in the Nyquist plot suggests that the mode of conduction in Sepia melanin is attributable to one type of charge carrier (i.e. electronic). EIS results would therefore agree with the *I–t* measurements, thus strengthening the hypothesis of predominant electronic transport for Sepia melanin. The presence of multiple semicircles would have been attributable to mixed electronic–ionic transport. The lack of a low-frequency capacitive tail indicates the absence of ionic transport and ion accumulation at the interface between Sepia melanin and the metal electrodes [15, 28]. The equivalent circuit in figure 3(B) includes R_c, the Sepia melanin/Au contact resistances, $R_{e,SM}$ the Sepia melanin resistance, and CPE_{geom}, the constant phase element denoting the system's geometrical capacitance. The dimensionless parameter α, ranging from

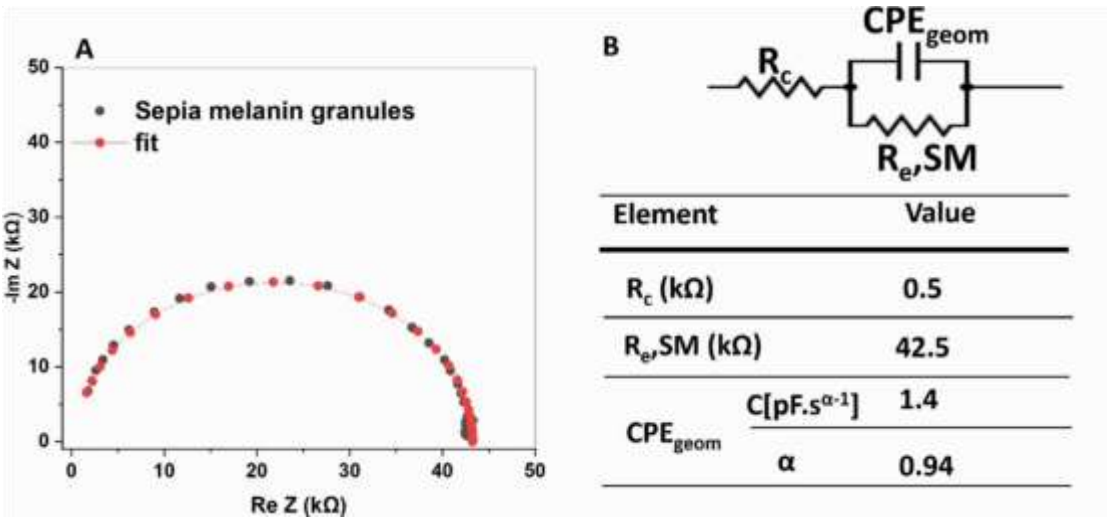

Element		Value
R_c (kΩ)		0.5
R_e,SM (kΩ)		42.5
CPE_{geom}	C[pF.s$^{\alpha-1}$]	1.4
	α	0.94

Figure3. EIS characterization of Sepia melanin granules, in ambient conditions: (A) Nyquist plot and (B) equivalent circuit model and table with extracted values.

0 to 1, quantifies the proximity of the element to a pure capacitor (in this last case, α= 1). We deduced for α a value of 0.94, close to the value for a pure capacitor.

Activation energy was extracted using the temperature-dependent *I–V* characteristics, measured in the range 295–380 K (figures 4(A) and (C) and SI, table S2), which show that the current increases with temperature. The logarithm of the conductivity plotted against the inverse of the temperature follows the Arrhenius law, with activation energy estimated at 60.2 ± 4.1 and 11.6 ± 2.0 meV, for samples with 700 and 400 nm interelectrode distance (figures S3(B) and (D)). The low activation energy suggests that trap states are shallow [29, 30]. Further, we tentatively suggest that the metal content in the Sepia melanin granules (due to the synthesis of Sepia melanin in natural environments, i.e. sea water) could create a doping-like condition [31].

In potentiostatic conditions, the increase of the temperature caused an increase in the value of the *plateau* current that can be described as $I = I_0 + m\,T$, where I_0 is the intercept with the *y*-axis and *m* is the slope of the plot (figures 4(B) and (D)), and SI, figures S3(A) and (C).

We decided to critically compare values of the conductivity of Sepia melanin obtained for different electrode spacings, available from our work and the literature (figure 5). We observed that the conductivity increases by decreasing the interelectrode distance. This increase is tentatively attributed to the decreased number of inter-granules' boundaries between Sepia melanin granules.

4. Conclusion

Natural organic electronic materials are of interest in sustainable organic electronics for their abundance and potential biodegradability. The Sepia melanin biopigment has been considered a prototype material in sustainable organic electronics. Since the hierarchical development of Sepia melanin brings about spherical granules with sizes approximately ranging between 100 and 300 nanometers, it is important to evaluate the electrical response at the nanoscale, to make a step ahead towards the discovery of the upper limit of the conductivity for Sepia melanin, expected to be in the inter-granules' boundary-free regime. This requires the use of EBL, considering that by conventional photolithography we can pattern interelectrode distances in the micrometric range. We propose the

general use of nanoscale electrodes for hierarchical nanostructured natural materials of interest in organic electronics.

SEM images show that granules form multi-granule structures whose length can bridge the interelectrode distances we probed during electrical characterizations (i.e. interelectrode distances of 400 nm and 700 nm, with electrodes patterned by EBL). Further, SEM images show that about 2 granules can bridge the interelectrode distance of 400 nm and about 4 granules can bridge the interelectrode distance of 700 nm. In the multi-granule structures observable in the SEM images, one granule interfaces one or more granules, i.e. granules share granules' boundaries (inter-granules' boundaries). We expect that such inter-granules' boundaries host charge carrier traps, detrimental to charge transport. It is important to observe that if the formation of the multi-granule structures is necessary for the formation of a conductive path bridging the interelectrode distance, inter-granules' boundaries within the multi-granule structures can host charge carrier traps that weaken transport. In agreement with that, we expected that lowering the number of inter-granules' boundaries is beneficial to transport (leading to an increase of the current). Our results show that the shorter interelectrode distance brings higher conductivity with respect to the longer one: the conductivity is $1.55 \pm 0.01 \times 10^{-2}$ S cm^{-1} for the interelectrode distance of 400 nm (with about one inter-granule boundary within the interelectrode distance) whereas the conductivity is $0.95 \pm 0.01 \times 10^{-2}$ S cm^{-1} for 700 nm (with about 3 inter-granules' boundaries within the interelectrode distance). We attribute the increase of the

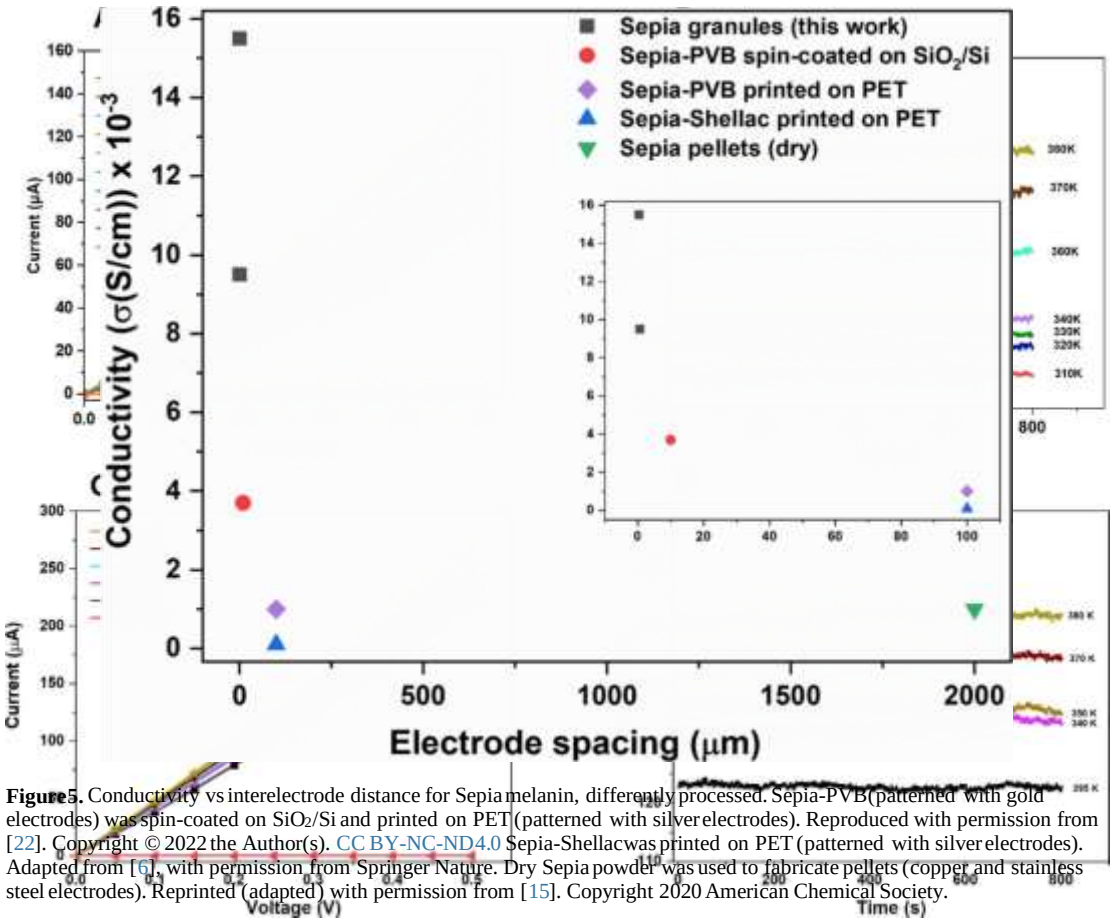

Figure5. Conductivity vs interelectrode distance for Sepia melanin, differently processed. Sepia-PVB(patterned with gold electrodes) was spin-coated on SiO_2/Si and printed on PET (patterned with silver electrodes). Reproduced with permission from [22]. Copyright © 2022 the Author(s). CC BY-NC-ND4.0 Sepia-Shellacwas printed on PET (patterned with silver electrodes). Adapted from [6], with permission from Springer Nature. Dry Sepia powder was used to fabricate pellets (copper and stainless steel electrodes). Reprinted (adapted) with permission from [15]. Copyright 2020 American Chemical Society.

Figure4. Temperature-dependent *I–V* and *I–t* characteristics of Sepia melanin granules at 0.3 V for the two interelectrode distances investigated in this work: 700 nm, (A) and (B), and 400 nm, (C) and (D).

conductivity with the decrease of the interelectrode distance to the lower number of inter-granules' boundaries within the interelectrode region in the former case with respect to the latter.

Current–time (potentiostatic) characteristics suggest that transport is predominantly electronic. Temperature-dependent current–voltage (*I–V*) measurements show an increase of the current with the temperature with transport activation energies of 60.2 and 11.6 meV, for distance ranges of 700 and 400 nm, respectively.

Work is in progress to further miniaturize the interelectrode distance to study inter-granules' boundary-free Sepia melanin, with the ultimate goal to discover the upper, intrinsic limit of its conductivity. This knowledge is required to design high-performance, biodegradable Sepia melanin-based electronics.

Data availability statement

All data that support the findings of this study are included within the article (and any supplementary files).

Acknowledgments

S K acknowledges financial support from MITACS for his PhD scholarship and CMC for microfabrication expenses. C S acknowledges NSERC (DG) and the Canada Research Chairs. We are

indebted to C Clement and M-H Bernier for their extraordinary technical support in and out of the clean room.

References

Baumgartner M *et al* 2017 Emerging “green” materials and technologies for electronics *Green Mater. Electron.* **101** 1–53

Birajdar M S, Joo H, Koh W-G and Park H 2021 Natural bio-based monomers for biomedical applications: a review *Biomater. Res.* **25** 8

Lemieux J, Belanger D and Santato C 2021 Toward biosourced materials for electrochemical energy storage: the case of tannins *ACS Sustain. Chem. Eng.* **9** 6079–86

Meredith P, Bettinger C J, Irimia-Vladu M, Mostert A B and Schwenn P E 2013 Electronic and optoelectronic materials and devices inspired by nature *Rep. Prog. Phys.* **76** 034501

Parker R M, Parton T G, Chan C L C, Bay M M, Frka-Petesic B and Vignolini S 2023 Bioinspired photonic materials from cellulose: fabrication, optical analysis, and applications *Acc. Mater. Res.* **4** 522–35

Camus A *et al* 2024 Electrical response and biodegradation of Sepia melanin-shellac films printed on paper *Commun. Mater.* **5** 173

Di Mauro E, Rho D and Santato C 2021 Biodegradation of bio-sourced and synthetic organic electronic materials towards green organic electronics *Nat. Commun.* **12** 3167

Nzihou A 2020 *Handbook on Characterization of Biomass, Biowaste and Related By-products* (Springer)

Society, E.C *Element Scarcity – EuChemS Periodic Table* 2023 (available at: www.euchems.eu/euchems-periodic-table/)

Torricelli F, Alessandri I, Macchia E, Vassalini I, Maddaloni M and Torsi L 2022 Green materials and technologies for sustainable organic transistors *Adv. Mater. Technol.* **7** 2100445

Zvezdin A, Di Mauro E, Rho D, Santato C and Khalil M 2020 En route toward sustainable organic electronics *MRS Energy Sustain.* **7** E16

Baldé C P *et al* 2024 *The Global E-waste Monitor. International Telecommunication Union (ITU)* (United Nations Institute for Training and Research (UNITAR)) pp 1–146

Gutowski T G, Branham M S, Dahmus J B, Jones A J, Thiriez A and Sekulic D P 2009 Thermodynamic analysis of resources used in manufacturing processes *Environ. Sci. Technol.* **43** 1584–90

d’Ischia M, Napolitano A, Pezzella A, Meredith P and Sarna T 2009 Chemical and structural diversity in eumelanins: unexplored bio-optoelectronic materials *Angew. Chem. Int. Ed.* **48** 3914–21

Reali M, Gouda A, Bellemare J, Ménard D, Nunzi J-M, Soavi F and Santato C 2020 Electronic transport in the biopigment sepia melanin *ACS Appl. Bio Mater.* **3** 5244–52

Wünsche J *et al* 2015 Protonic and electronic transport in hydrated thin films of the pigment eumelanin *Chem. Mater.* **27** 436–42

Cheng J, Moss S C and Eisner M 1994 X-ray characterization of melanins—II *Pigment Cell Res.* **7** 263–73

Niyonkuru D, Camus A, Reali M, Gao Z, Shadrack D M, Butyaev O, Surtchev M and Santato C 2023 A nanoscale study of the structure and electrical response of Sepia eumelanin *Nanoscale Adv.* **5** 5295–300

McGinness J, Corry P and Proctor P 1974 Amorphous semiconductor switching in melanins *Science* **183** 853–5

Mostert A B, Powell B J, Pratt F L, Hanson G R, Sarna T, Gentle I R and Meredith P 2012 Role of semiconductivity and ion transport in the electrical conduction of melanin *Proc. Natl Acad. Sci.* **109** 8943–7

Mostert A B, Rienecker S B, Noble C, Hanson G R and Meredith P 2018 The photoreactive free radical in eumelanin *Sci. Adv.* **4** eaaq1293

Camus A, Reali M, Rozel M, Zhuldybina M, Soavi F and Santato C 2022 High conductivity Sepia melanin ink films for environmentally benign printed electronics *Proc. Natl Acad. Sci.* **119** e2200058119

Magarelli M, Passamonti P and Renieri C 2010 Purification, characterization and analysis of sepia melanin from commercial sepia ink (Sepia Officinalis) *Rev. CES Med. Vet. Zoot.* **5** 18 – 28

Osak W, Tkacz K, Czternastek H and Sławinski´ J 1989 I–V characteristics and electrical conductivity of synthetic melanin *Biopolymers* **28** 1885–90

Haneef H F, Zeidell A M and Jurchescu O D 2020 Charge carrier traps in organic semiconductors: a review on the underlying physics and impact on electronic devices *J. Mater. Chem. C* **8** 759–87

Rose A 1955 Space-charge-limited currents in solids *Phys. Rev.* **97** 1538

Salleo A 2013 Electronic traps in organic semiconductors *Organic Electronics* (Wiley) 341–80

Huggins R A 2002 Simple method to determine electronic and ionic components of the conductivity in mixed conductors a review *Ionics* **8** 300–13

Jastrzebska M, Kocot A and Tajber L 2002 Photoconductivity of synthetic dopa–melanin polymer *J. Photochem. Photobiol. B* **66** 201–6

Jastrzebska M M, Isotalo H, Paloheimo J and Stubb H 1996 Electrical conductivity of synthetic DOPA-melanin polymer for different hydration states and temperatures *J. Biomater. Sci. Polym. Ed.* **7** 577–86

Mostert A B, Rienecker S B, Sheliakina M, Zierep P, Hanson G R, Harmer J R, Schenk G and Meredith P 2020 Engineering proton conductivity in melanin using metal doping *J. Mater. Chem. B* **8** 8050–60